Magnetic Resonance in Medicine 71:230–237 (2014)

Triple Echo Steady-State (TESS) Relaxometry

Rahel Heule,[1]* Carl Ganter,[2] and Oliver Bieri[1]

Purpose: Rapid imaging techniques have attracted increased interest for relaxometry, but none are perfect: they are prone to static (B_0) and transmit (B_1) field heterogeneities, and commonly biased by T_2/T_1. The purpose of this study is the development of a rapid T_1 and T_2 relaxometry method that is completely (T_2) or partly (T_1) bias-free.

Methods: A new method is introduced to simultaneously quantify T_1 and T_2 within one single scan based on a triple echo steady-state (TESS) approach in combination with an iterative golden section search. TESS relaxometry is optimized and evaluated from simulations, in vitro studies, and in vivo experiments.

Results: It is found that relaxometry with TESS is not biased by T_2/T_1, insensitive to B_0 heterogeneities, and, surprisingly, that TESS-T_2 is not affected by B_1 field errors. Consequently, excellent correspondence between TESS and reference spin echo data is observed for T_2 in vitro at 1.5 T and in vivo at 3 T.

Conclusion: TESS offers rapid T_1 and T_2 quantification within one single scan, and in particular B_1-insensitive T_2 estimation. As a result, the new proposed method is of high interest for fast and reliable high-resolution T_2 mapping, especially of the musculoskeletal system at high to ultra-high fields. **Magn Reson Med 71:230–237, 2014. © 2013 Wiley Periodicals, Inc.**

Key words: triple echo steady-state; relaxometry; fast imaging; T_1; T_2; quantification

Since its introduction more than half a century ago, the use of steady-state free precession (SSFP) (1) has become increasingly popular, and a large number of SSFP imaging techniques has been described so far (e.g., see Handbook of MRI Pulse Sequences (2). Besides morphological imaging, SSFP has also attracted considerable interest for fast quantitative MRI. Quantitative imaging is thought to represent an important future step toward a significant improvement of the diagnostic potential of MRI, for the early detection of subtle or diffuse pathological changes with high specificity and sensitivity, for an unbiased assessment of treatment or drug effects, as well as for clinical trials in drug research across different sites. When compared with morphological imaging, however, quantification requires longer scan time and the overall success and applicability of quantitative MRI methods in the clinical setting will depend greatly on the overall acquisition speed. As a result, SSFP-based imaging techniques have come into the research focus, e.g., for relaxation time mapping (3–10), for measuring molecular proton diffusion (11–15), for the assessment of magnetization transfer effects (16–18), or for the characterization of flow or motion (19–21).

Relaxation is one of the most fundamental fingerprints of NMR. It not only defines contrast in conventional MRI but also reflects the local interaction of water on a molecular and thus very fundamental level. Longitudinal relaxation (T_1) is typically assessed from inversion recovery (IR) spin echo (SE) techniques, whereas transverse relaxation (T_2) is commonly based on sampling the decay of the transverse magnetization using single-echo or multiecho SE methods. Acquiring the complete T_1 recovery or T_2 decay curve is time consuming and frequently requires segmented imaging strategies. In contrast, quantification techniques that make use of the functional dependence of the steady state on its intrinsic and extrinsic parameters are considerably faster. A common feature of rapid SSFP sequences is their mixed T_2/T_1 imaging contrast; a natural consequence of a pulse repetition time (TR) being much shorter than T_2. As a result, accurate quantification of relaxation times using SSFP-based imaging techniques is hampered by a varying marginal T_2-related bias in T_1 estimates, as seen in radiofrequency spoiled SSFP (22), or by a more or less pronounced T_1-related bias in T_2, as seen in balanced SSFP (23), partially spoiled SSFP (10), and double echo SSFP (9). Moreover, all SSFP imaging techniques proposed so far, as well as multiecho SE techniques commonly used for T_2 mapping, are highly sensitive to transmit field (B_1) inhomogeneities that become especially prominent at high (3 T) to ultra-high (7 T and higher) field strength. As a result, without additional corrective data, accurate and thus fast and reliable quantification of relaxation times is not feasible in practice.

In summary, several different steady-state methods have been proposed for relaxometry, but none are perfect: all of them are B_1-sensitive, require multiple scans (except for the dual echo approach (9)), suffer from a T_2/T_1 related bias, or are prone to static (B_0) field inhomogeneities (24). Hence, there is much room for methodological improvement. In this work, we present a completely new approach for rapid quantification of both, T_1 and T_2 relaxation times, within one single scan using a triple echo steady-state (TESS) approach. Here, we make use of the different functional dependence of the two lowest order SSFP-FID modes (free induction decay) and of the lowest order SSFP-Echo mode, acquired within every TR, for rapid relaxometry using an iterative golden section search algorithm. The accuracy of TESS-based

[1]Division of Radiological Physics, Department of Radiology, University of Basel Hospital, Basel, Switzerland.

[2]Department of Radiology, Klinikum rechts der Isar, Technische Universität München, Munich, Germany.

Grant sponsor: Schweizerischen Nationalfonds; Grant number: SNF 325230-132906.

*Correspondence to: Rahel Heule, M.Sc., Division of Radiological Physics, Department of Radiology, University of Basel Hospital, Petersgraben 4, 4031 Basel, Switzerland. E-mail: rahel.heule@unibas.ch

Received 1 October 2012; revised 27 December 2012; accepted 4 January 2013

DOI 10.1002/mrm.24659
Published online 2 April 2013 in Wiley Online Library (wileyonlinelibrary.com).

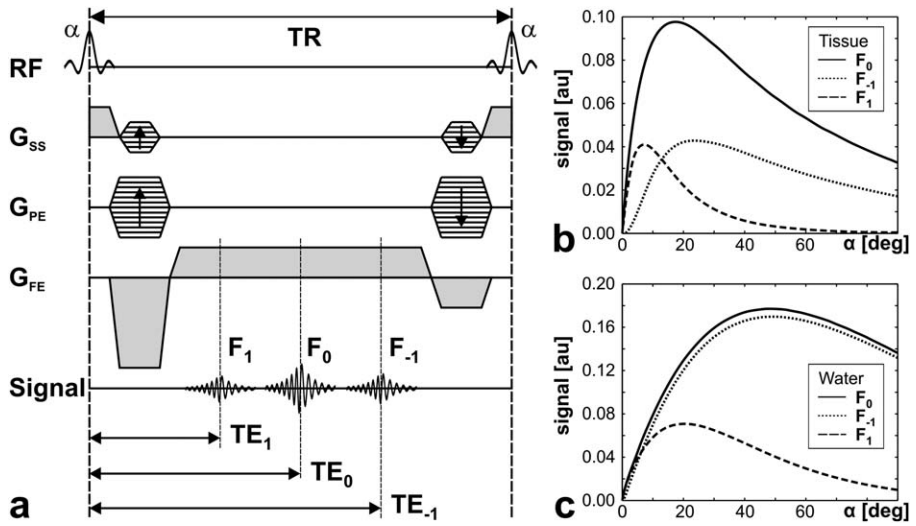

FIG. 1. (**a**) Illustration of a triple echo steady-state (TESS) sequence. The center free induction decay (FID) (F_0) is flanked by a higher order FID to the left (F_1) and by the lowest order Echo (F_{-1}) to the right, with echo times TE_0, TE_1, and TE_{-1}, respectively. (**b** and **c**) Simulated TESS signals for tissues (b) and water (c) as a function of the flip angle α. Simulation parameters: $TR = 16$ ms, $TE_1 = TE_0 \rightarrow 0$, and $TE_{-1} \rightarrow$ TR, tissues: $T_1/T_2 = 1000$ ms/50 ms, water: $T_1/T_2 = 3000$ ms/1000 ms.

relaxometry is evaluated from simulations and in vitro experiments, and the feasibility of high-resolution three-dimensional (3D) T_1 and T_2 mapping is presented in vivo for human articular cartilage at 3 T.

METHODS

All numerical simulations, data analysis, and visualization were done using Matlab 7.5 (The MathWorks, Inc., Natick, MA). Measurements and calibrations were performed on a clinical 1.5 T and a 3 T system equipped with actively shielded magnetic field gradient coils.

Triple Echo Steady State

Multiecho SSFP, as displayed in Figure 1a, was already proposed by Mizumoto and Yoshitome for imaging different contrast dependencies (25). Generally, the ideal SSFP signal (no motion, no diffusion, quasi-instantaneous radiofrequency pulses) can be written in a representation that is closely related to configuration theory (26). Expressions for the two lowest order modes (F_0, representing the FID, and F_{-1} representing the Echo) immediately following the excitation pulse can be found, e.g., in (27),

$$F_0 \propto 1 - (E_1 - \cos\alpha) \cdot r \qquad [1]$$

$$F_{-1} \propto (1 - (1 - E_1\cos\alpha) \cdot r)E_2^{-1} \qquad [2]$$

with definitions

$$E_{1,2} := \exp\left(-TR/T_{1,2}\right)$$

$$p := 1 - E_1\cos\alpha - {E_2}^2(E_1 - \cos\alpha)$$

$$q := E_2(1 - E_1)(1 + \cos\alpha)$$

$$r := \left(1 - E_2^2\right)\left(p^2 - q^2\right)^{-1/2}$$

All higher order modes can then be derived from F_0 and F_{-1} as

$$F_n = \begin{cases} \left(\frac{u_1}{u_0}\right)^n \cdot F_0 & for \quad n \geq 0 \\ \left(\frac{u_1}{u_0}\right)^{|n|-1} \cdot F_{-1} & for \quad n < 0 \end{cases} \qquad [3]$$

using

$$u_0 := p\left(p^2 - q^2\right)^{-1/2}, u_1 := \frac{p}{q}(u_0 - 1)$$

For the F_1 mode, we thus find

$$F_1 \propto q^{-1} \cdot \left(p - \sqrt{p^2 - q^2}\right) \cdot (1 - (E_1 - \cos\alpha) \cdot r) \qquad [4]$$

Note that all modes F_n in Eq. [3] are positive by definition (in contrast to Eq. 21 given in Ref. 27, where the modes are negative for $n < 0$). Exemplary F_1, F_0, and F_{-1} steady-state signal levels for tissues and fluids are shown in Figure 1b,c as a function of the flip angle. Taking now into account that the signals are acquired with $t > 0$ (rather than $t = 0$), the signal expressions become weighted by the corresponding echo time (TE_1, TE_0, and TE_{-1}; for details, see Fig. 1a)

$$F_{1,0,-1} \rightarrow F_{1,0,-1} \times \exp\left(-\mathrm{TE}_{1,0,-1}/T_2\right) \qquad [5]$$

For short enough TEs, a T_2 rather than a T_2^* weighting is introduced to Eqs. [1], [2], and [4]. As reported in (28), the error arising from such an approximation is small.

Relaxometry With TESS

As proposed for rapid quantification of T_2 from double echo steady state (DESS) (9), we follow the initial idea of exploiting the dependencies of the modes on relaxation to quantify T_1 and T_2. To this end, we investigate the following signal ratios (see Fig. 2):

$$s_{T_2}(T_1) := \frac{F_1}{F_0}, \quad s_{T_1}(T_2) := \frac{F_{-1}}{F_0 - F_1} \qquad [6]$$

Here, the subscript T_2 (T_1) is used to indicate that for the ratio $s_{T_2}(T_1)$ ($s_{T_1}(T_2)$) the relaxation time T_2 (T_1) is

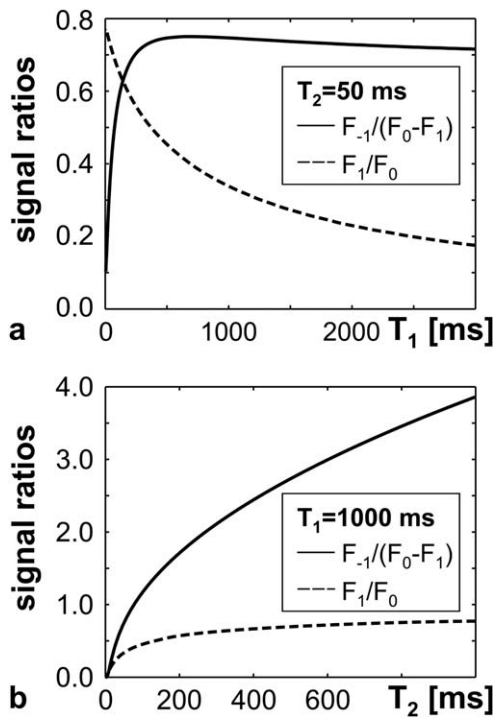

FIG. 2. Simulation of relevant signal ratios (s_{T_1}, s_{T_2}) according to Eq. [6] using a flip angle of 15°, derived from the three base modes, as acquired with TESS (see Fig. 1). (**a**) Signal ratios as a function of T_1 for a fixed T_2 of 50 ms. Only the F_1/F_0 signal ratio shows a bijective behavior and a good sensitivity for $T_2 << T_1$. (**b**) Signal ratios as a function of T_2 for a fixed T_1 of 1000 ms. Only the $F_{-1}/(F_0 - F_1)$ signal ratio is sensitive to the limit of $T_2/T_1 \rightarrow 1$.

considered to be a bound variable: formally, the signal ratios then depend for any given set of extrinsic parameters (TR, $TE_{1,0,-1}$, and α) only on one running variable, namely, T_1 or T_2.

From this, an easy and fast iterative procedure based on a one-dimensional numerical minimization can be used for the derivation of T_1 and T_2, as described in the following: A search interval for T_1 and T_2 with a (dummy) upper guess of $T_{1,u} = T_{2,u} = 5$ s is defined. The iteration is initialized with a global estimate for the longitudinal relaxation time, $T_{1,i=0} \in [0, T_{1,u}]$, and a golden section search (29) performed to calculate an estimate for the transverse relaxation time, $T_{2,i+1}$, based on the measured signal ratio s_{T_1} (see Eq. [6]),

$$T_{2,i+1} = \arg\min \left\{ T_2 \in [0, T_{2,u}] : \left| s_{T_1,\text{meas}} - s_{T_{1,i}}(T_2) \right| \right\} \quad [7]$$

Now, the obtained guess of $T_{2,i+1}$ is used to yield an improved $T_{1,i+1}$ estimate based on the signal ratio s_{T_2} (see Eq. [6]), according to

$$T_{1,i+1} = \arg\min \left\{ T_1 \in [0, T_{1,u}] : \left| s_{T_2,\text{meas}} - s_{T_{2,i+1}}(T_1) \right| \right\} \quad [8]$$

again using a golden section search, but now on T_1. The improved $T_{1,i+1}$ estimate can then be used again to calculate an updated $T_{2,i+2}$ estimate based on Eq. [7], and so on. The iteration stops as soon as the change in both T_1 and T_2 is less than a user defined convergence tolerance, i.e., 0.1 ms. While iterating, the whole search procedure becomes independent of the initial T_1 estimate. In this work, we use a consistent rough global estimate of $T_1 = 1000$ ms for all simulations, as well as in vitro and in vivo relaxometry. Even with such a rough guess, typically less than 10 iterations are required for convergence of the algorithm.

The specific choice of the signal ratios given in Eq. [6] is motivated as follows: Instead of the basic ratio F_{-1}/F_0 which is used with DESS for T_2 quantification, we investigate the ratio $F_{-1}/(F_0 - F_1)$, because it shows a stronger sensitivity to T_2 (see Fig. 2b where the good T_2-sensitivity of this ratio is apparent). For T_1 estimation using TESS, another independent ratio is required and we choose F_1/F_0 because of its strong sensitivity to T_1 (see Fig. 2a). The investigated signal ratios necessarily have to be bijective functions of either T_1 or T_2. More precisely, $s_{T_2}(T_1)$ ($s_{T_1}(T_2)$) has to be bijective with respect to T_1 (T_2) which holds for our choice. Otherwise, the minimization might run into local rather than global minima.

Simulations

Optimal signal-to-noise ratio (SNR) is not only achieved at different flip angles for different modes but also depends on relaxation times (see Fig. 1b,c). We aim at finding optimal flip angle settings for TESS-based relaxometry and analyze the impact of noise on the T_1 and T_2 calculation. To this end, a Monte-Carlo simulation is performed for a range of idealized homogeneous T_2/T_1-probes with signal amplitudes according to Eqs. [1–5]. Optimal flip angle settings are explored based on 100,000 $F_{1,0,-1}$ drawings with mean zero and $0.001M_0$ standard deviation. The value of the standard deviation directly relates to the amount of noise in the acquired MR images. From the sample of noisy signal amplitudes, distributions of $T_{1,2}$ with mean $<T_{1,2}>$ and standard deviation $\Delta T_{1,2}$ are calculated based on Eqs. [6–8]. The SNR for relaxation time mapping using TESS can then be estimated from $\text{SNR}_{T_1,T_2} := <T_{1,2}>/\Delta T_{1,2}$. Relative SNR is evaluated according to $\text{rSNR}_{T_1,T_2} := \text{SNR}_{T_1,T_2}/\max\{\text{SNR}_{T_1},\text{SNR}_{T_2}\}$ for flip angles ranging from 5° to 40° and for T_2/T_1 ratios ranging from 0.01 to 1.0, using logarithmically spaced T_2 values between 10 ms and 1000 ms, but a fixed T_1 of 1000 ms.

Measurements

A contemporary DESS sequence was adapted for acquisition of F_1, F_0, and F_{-1} within every TR, as displayed in Figure 1a. Generally, although not limited to, the same bandwidth was used for the acquisition of all echoes. To provide enough SNR in the base data for T_1 and T_2 calculation, some averages of the TESS scan were taken as specified below.

In vitro relaxation time mapping with TESS was performed at 1.5 T using manganese-doped spherical phantoms (0 mM, 0.05 mM, 0.125 mM, 0.25 mM, 0.5 mM $MnCl_2$ in H_2O) of about 14 cm in diameter. Longitudinal relaxation was assessed from single-slice IR turbo spin

echo (TSE) experiments with inversion times ranging between 25 ms and 9.6 s. For a single IR-TSE scan with 2.5 × 2.5 mm^2 in-plane resolution (128 × 64 matrix) and 5 mm slice thickness, using a turbo factor of 7, a TR of 10 s, a TE of 12 ms, and a bandwidth of 130 Hz/pixel, image acquisition was completed within 1 min 22 s. Transverse relaxation was measured from a contemporary single-echo SE method with a TE ranging from 5 ms up to 3.2 s. One single scan was completed within 3 min 18 s, yielding 2.5 × 5.0 mm^2 in-plane resolution (128 × 32 matrix) and 5 mm slice thickness, using a turbo factor of 1, a TR of 6 s, and a bandwidth of 592 Hz/pixel. A single-echo rather than a multiecho approach was used to avoid any possible bias in T_2 from stimulated echo contributions (30). TESS imaging was performed in 3D with 4 mm isotropic resolution (64 × 64 × 44 matrix). Scans were performed with a nominal flip angle of 40° and a constant bandwidth of 240 Hz/pixel for all three echoes, yielding an overall TR of 15.7 ms with corresponding $TE_1 = 3.6$ ms, $TE_0 = 8.0$ ms, and $TE_{-1} = 12.4$ ms. Four averages were taken and the 3D TESS scan was completed within 2 min and 58 s.

In vivo human knee scans at 3 T of two healthy volunteers were performed with 3D TESS in axial and sagittal orientation (the slab consisted of 12 slices with 3 mm resolution) using a dedicated 15-channel transmit and receive knee coil (QED) yielding 0.6 × 0.6 mm^2 in-plane resolution (256 × 232 × 18 image encoding matrix). Imaging was performed with water-selective excitation pulses ($1\bar{2}1$-binomials) of nominal 15° flip angle. The bandwidth was set to 230 Hz/pixel, yielding a TR of 20.6 ms, and corresponding echo times $TE_1 = 6.6$ ms, $TE_0 = 11.0$ ms, and $TE_{-1} = 15.4$ ms. Seven averages were taken. The 3D TESS scan was completed within 4 min and 24 s. Reference T_1 values were calculated from six consecutive IR-TSE scans (12 slices, 0.3 mm gap, 2.7 mm slice thickness, 0.6 × 0.6 mm^2 in-plane resolution using a 256 × 232 matrix, turbo factor 8, a TR of 6 s, a TE of 10 ms, and a bandwidth of 227 Hz/pixel) with inversion times ranging between 25 ms and 2.35 s. A single scan took 1 min 44 s to complete. Reference T_2 values were derived based on nine consecutive single-echo SE scans (12 slices, no gap, 3 mm slice thickness, 0.6 × 0.6 mm^2 in-plane resolution using a 256 × 232 matrix, turbo factor 1, a TR of 1210 ms, and a bandwidth of 227 Hz/pixel) with corresponding TEs of 10, 20, 30,..., 90 ms. One single-echo SE scan was completed within 2 min 39 s. For comparison, a multiecho SE approach (nine echoes: starting from 10 ms, and having an echo spacing of 10 ms) was also used with identical settings as the single-echo scan.

RESULTS

Relaxometry based on TESS is exemplarily illustrated in Figure 3 at 1.5 T for one of the manganese-doped spherical probes (0.25 mM $MnCl_2$ in H_2O) with a nominal T_1 of 456 ms and a nominal T_2 of 48.5 ms, derived by SE techniques (see "Methods" section for details) and regarded in the following as gold standard (31). From a single 3D TESS scan, three different sets of images are acquired (see also Fig. 1a) with formal descriptions as stated in Eqs. [1–5]. From the s_{T_1} signal ratio (see Eq. [6]), an estimated T_2 value is found (using Eq. [7], and an initial estimate of $T_{1,0} = 1$ s). The obtained value is then used to calculate an updated estimate of T_1, based on s_{T_2} (see Eqs. [6] and [8]). This procedure is repeated until the iterative change in T_1 and T_2 falls below a certain threshold (here, 0.1 ms). Typically, the iterative procedure converges very quickly (see Fig. 3). The resulting T_1 and T_2 maps are also shown in Figure 3, with the relaxometry results summarized in Table 1 for all probes (evaluated for a circular region of interest, placed in the center of the phantoms as indicated in Fig. 3). Generally, excellent agreement is found between reference single-echo SE and TESS transverse relaxometry data. However, some variation is observed for T_1 using TESS. Interestingly, no spatial variation can be seen for T_2, whereas T_1 decreases by about 20% toward the rim of the phantom.

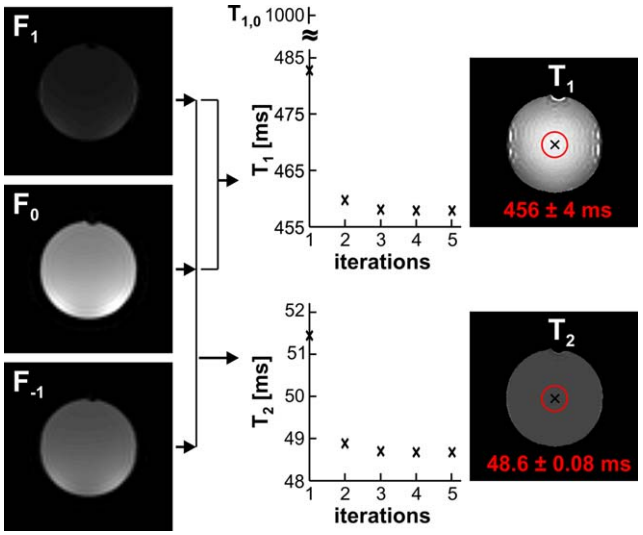

FIG. 3. Illustration of iterative relaxometry calculations from F_1, F_0, and F_{-1} base images, as presented in Eqs. [7] and [8]. The iteration is exemplarily shown for a pixel in the center of the phantom (black cross). Based on the s_{T_1} signal ratio (with an initial guess of $T_{1,0} = 1$ s), a guess of $T_{2,1} \sim 51.5$ ms is derived from Eq. [7] using a golden section search. This first guess of T_2 is then used to find an updated estimate of $T_{1,1} \sim 483$ ms based on Eq. [8], again using a golden section search. This procedure is repeated until the change in both T_1 and T_2 falls below a certain threshold (here, 0.1 ms); typically, requiring less than 10 iterations. Relaxation parameters were assessed for a region of interest, as indicated in the relaxation maps by the circle. [Color figure can be viewed in the online issue, which is available at wileyonlinelibrary.com.]

The spatial variation of T_1, as observed in vitro (see Fig. 3), is likely to be due to B_1 field heterogeneities

Table 1
In Vitro Comparison of Single-Echo Spin Echo and TESS Relaxometry Data (T_1 and T_2) on Manganese-Doped Aqueous Probes at 1.5 T (for Protocol Details, see "Methods" Section)

	TESS	IR-SE	TESS	SE
[$MnCl_2$]	T_1 (ms)	T_1 (ms)	T_2 (ms)	T_2 (ms)
0.000 mM	3208 ± 126	2995 ± 2	2082 ± 79	1903 ± 7
0.050 mM	1481 ± 12	1485 ± 2	240 ± 1.0	241 ± 1.1
0.125 mM	871 ± 10	858 ± 1	104.0 ± 0.27	104.7 ± 0.28
0.250 mM	456 ± 4	456 ± 1	48.6 ± 0.08	48.5 ± 0.17
0.500 mM	263 ± 2	272 ± 1	27.0 ± 0.02	27.0 ± 0.11

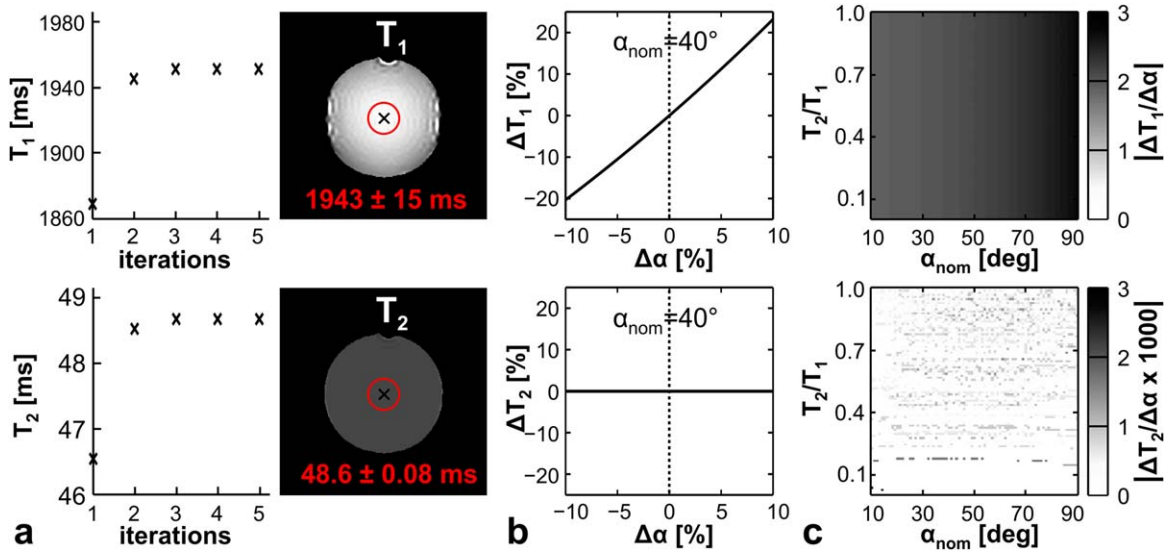

FIG. 4. (**a**) Recalculation of T_1 and T_2, as presented in Figure 3, but using only half of the nominal flip angle for the calculation, i.e., 20°, instead of 40°. As a result of the dramatic underestimation of the actual flip angle by 50%, T_1 is considerably overestimated (1943 ms, instead of 456 ms), but exactly the same value is derived for T_2. (**b**) B_1-sensitivity of T_1 (top) and T_2 (bottom) simulated for the flip angle and relaxation times of the phantom shown in (a). (**c**) Simulated B_1-sensitivity, as shown in (b), over a complete range of flip angles and T_2/T_1 times. Note the different scales in the sensitivity maps for T_1 and T_2. [Color figure can be viewed in the online issue, which is available at wileyonlinelibrary.com.]

and thus related to a miscalibration between the nominal (α_{nom}) and the actual flip angle (α_{act}) in the probes. This is confirmed by rerunning the calculation, but this time assuming a halved excitation angle, that is with $\alpha_{nom} = 20°$, instead of $\alpha_{nom} = 40°$. As a result, a strongly falsified T_1 is observed (see Fig. 4a); however, T_2 proves to be completely inert. The sensitivity to transmit field errors, $\Delta\alpha := (\alpha_{act} - \alpha_{nom})/\alpha_{nom}$, is now systematically evaluated, as exemplarily demonstrated in Figure 4b for $\alpha_{nom} = 40°$ and $T_1/T_2/TR = 456$ ms/48.5 ms/16 ms. The B_1-sensitivity of T_1, $\Delta T_1/\Delta\alpha$, is about 2, but $\Delta T_2/\Delta\alpha$ is barely noticeable, where $\Delta T_{1,2} := (T_{1,2}(\alpha_{act}) - T_{1,2}(\alpha_{nom}))/T_{1,2}(\alpha_{nom})$. This surprising result is not a remarkable coincidence related to a lucky choice of relaxation and sequence parameters, but can be confirmed over a large range of relaxation parameters and flip angles (Fig. 4c). Thus, TESS offers a unique opportunity for fast, accurate, and unbiased T_2 quantification, whereas T_1 estimates show the expected typical prominent sensitivity of contemporary steady-state methods to B_1 field errors, requiring corrective data. The atypical behavior of TESS-T_2 is of special advantage and benefit in vivo.

For high-resolution in vivo TESS relaxometry, SNR is expected to become critical and propagation of noise must be evaluated. Corresponding simulation results are shown in Figure 5. The expected relative SNR for T_1 (Fig. 5a) and T_2 (Fig. 5b) mapping using TESS is strongly affected by the choice of the flip angle (as might already be expected from the corresponding signal curves, see Fig. 1b,c). Generally, a pronounced relative SNR maximum can be observed in both T_1 and T_2 near $\alpha \sim 15°$ with respect to a $T_2/T_1 \sim 0.05$–0.1, that is, for tissues. As a result, optimal SNR for TESS-based relaxometry can be achieved in the low flip angle and low T_2/T_1 limit.

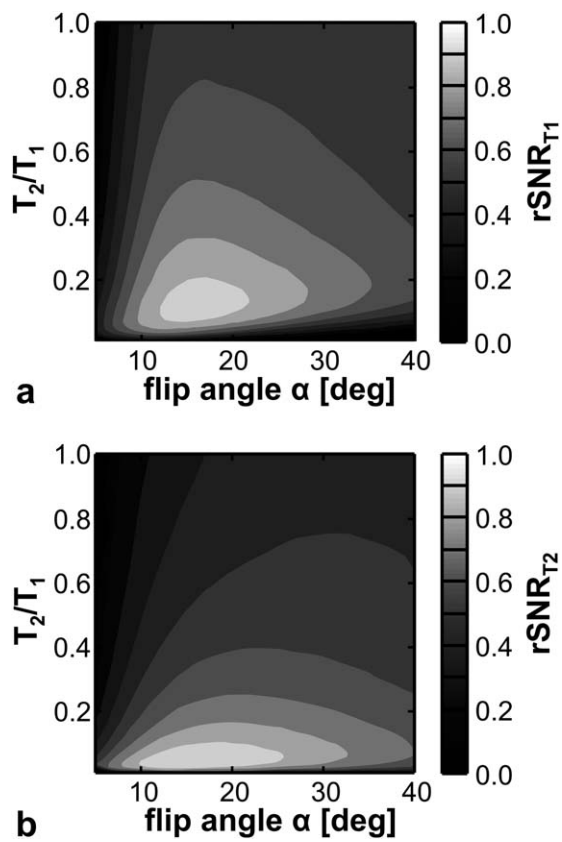

FIG. 5. Monte-Carlo simulation of the relative SNR for TESS relaxometry as a function of the flip angle and relaxation times ($T_2 = 10$–1000 ms, $T_1 = 1000$ ms) for a TR of 16 ms (for simulation details, see "Methods" section). (**a**) Relative SNR for T_1 mapping ($rSNR_{T_1}$). (**b**) Relative SNR for T_2 mapping ($rSNR_{T_2}$).

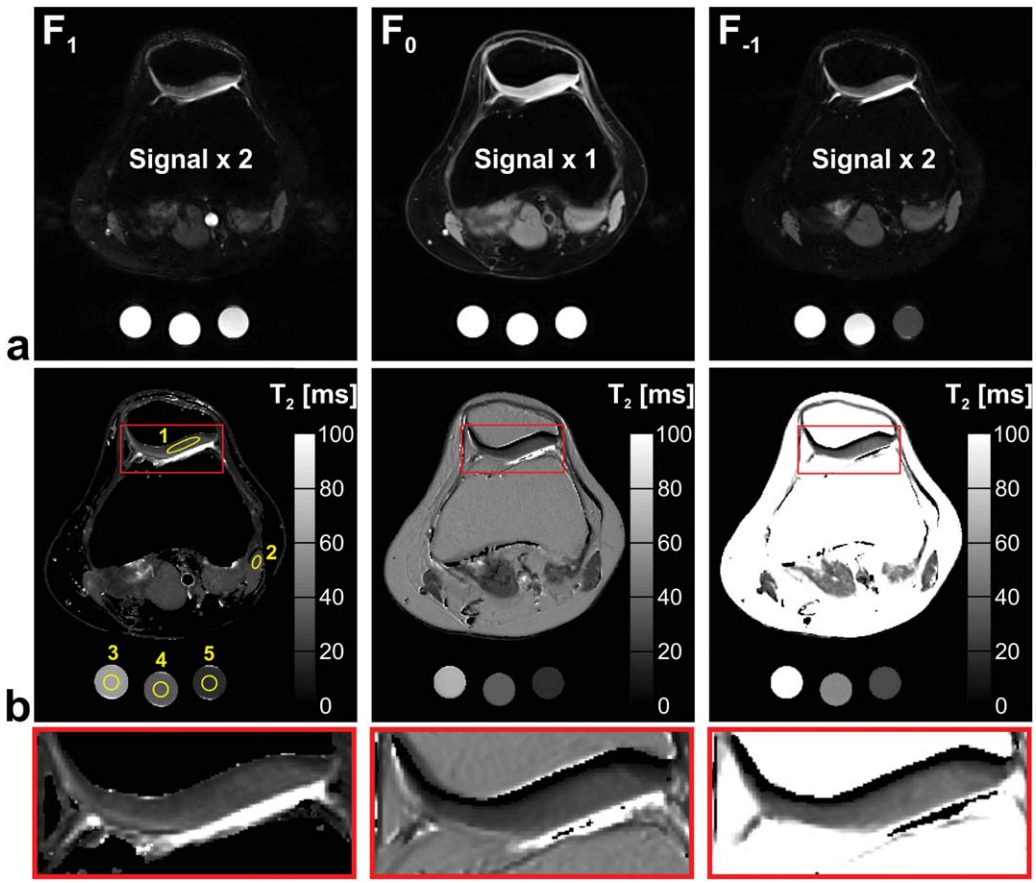

FIG. 6. (**a**) Exemplary axial TESS base images (F_1, F_0, and F_{-1}) of the knee joint at 3 T obtained with water-selective excitation pulses. For better visibility, the signals corresponding to the F_1 and F_{-1} mode were multiplied by a factor of 2. (**b**) T_2 values derived either by TESS (left), or by using a single-echo SE approach (middle), or by using a multiecho SE method (right). The manganese-doped test tubes (0.125 mM, 0.25 mM, and 0.5 mM) serve as internal controls. For selected regions of interest (indicated by the yellow numbers), T_2 values are summarized in Table 2. Again, excellent correspondence is observed in T_2 between TESS and single-echo SE data (see also Table 1), whereas the multiecho SE approach shows a clear overestimation of T_2 from stimulated echo contributions.

High-resolution in vivo 3D TESS relaxometry is demonstrated in the knee joint at 3 T in axial (Fig. 6) and sagittal (Fig. 7) slice orientation using optimal flip angles for tissues. As an internal control, three small test tubes containing 0.125 mM, 0.25 mM, and 0.5 mM $MnCl_2$ were placed adjacent to the knee for the axial scan. B_1-insensitive TESS-T_2 quantification is illustrated in Figure 6 and compared with reference T_2 maps calculated based on single-echo and multiecho SE experiments. Transverse relaxation time values are assessed for selected regions of interest (for definition of regions of interest, see Fig. 6) with corresponding results summarized in Table 2. Overall, excellent correspondence between TESS and single-echo SE transverse relaxometry data is found, whereas T_2 values, derived from multiecho SE data, show a pronounced overestimation of about 30–40% for cartilage, muscle, and for the internal controls due to stimulated echo contributions (from imperfect refocusing pulses and thus due to B_1 errors).

The distinct B_1-insensitivity of TESS-T_2 becomes especially apparent in the sagittal T_2 scan (Fig. 7b) where no variation in muscle-T_2 can be observed over the complete field of view. This is quite contrary to the corresponding TESS-T_1 map (Fig. 7c, right). It appears more inhomogeneous and shows clearly visible variations in muscle-T_1 over the field of view originating from B_1 heterogeneities. Comparison of TESS-T_1 with a reference measurement based on six consecutive IR-TSE scans (Fig. 7c, left) reveals that the T_1 map calculated with TESS is flawed as expected. However, good correspondence can be observed in regions where B_1 field errors are not that prominent, for instance in the patella: There, TESS relaxometry yields a T_1 of 869 ± 45 ms for the region of interest indicated by the arrow in Figure 7c compared with a T_1 of 839 ± 40 ms obtained with IR-TSE.

DISCUSSION

A variety of SSFP methods have been proposed thus far and are known in the literature for fast relaxometry, but all of them are sensitive to B_1 and show some more or less pronounced mixed T_2/T_1-sensitivity that can be mitigated by companion scans. As a result, without the use of additional corrective data, current SSFP techniques fail

to deliver accurate, reliable, and stable quantification results.

In this work, we report on a similar approach, as proposed for rapid T_2 quantification of cartilage using DESS imaging (28,32). In the limit of $\alpha \sim 90^\circ$, the ratio between the F_{-1} and F_0 signal, as acquired with DESS, becomes independent of T_1, allowing accurate quantification of T_2 (9). Signal-to-noise, however, is especially poor in this limit, requiring considerably lower flip angles in practice and, hence, leading to a systematic T_1-related bias in the estimated T_2 values using DESS. In principle, we solve this issue by acquiring a third independent mode, namely, F_1. Based on two independent signal ratios, the interacting T_1- and T_2-sensitivity can be tackled by a simple and fast ping-pong approach, using a golden section search, until the calculated signal ratios converge to the actual measured ones. As a result, TESS offers the possibility of acquiring both T_1 and T_2 within one single scan and without the confounding influence of either T_1 on T_2 or T_2 on T_1 (as observed with any other steady-state method). Moreover, from the application of crusher gradients within every TR, TESS is not affected by static field inhomogeneities. However, some motion sensitivity must be taken into account. Therefore, proper fixation seemed mandatory and was carefully conducted before every measurement. Diffusion effects are expected to be negligible for tissues, but reduce the signal of fluids for high-resolution scans (33).

As with any other fast quantitative SSFP imaging technique, TESS-based relaxometry is expected to be affected by B_1 field heterogeneities, and the impact of such transmit field calibration errors on T_1 and T_2 quantification was analyzed in Figure 4. Surprisingly, T_2 relaxometry with TESS revealed to be independent of B_1, whereas T_1 quantification showed the expected pronounced B_1-related estimation errors. This extraordinary feature is not only of special interest for high to ultra-high field T_2 relaxometry where prominent B_1 variations can be expected and applicability of SE techniques might be limited due to SAR constraints but also provides accurate quantification results in combination with spectral-spatial excitation pulses that typically entail flip angle calibration errors in the presence of B_0 heterogeneities. Spectral-spatial excitation, as demonstrated in Figures 6 and 7 for TESS, is especially beneficial for musculoskeletal imaging where fat is often found adjacent or interspersed within the tissues of interest. Fat suppression may thus not only enhance diagnostic information (34) but also eliminates the chemical shift artefact and thereby allows readout of the SSFP signal modes with a reduced receiver bandwidth which in turn results in an overall increased SNR.

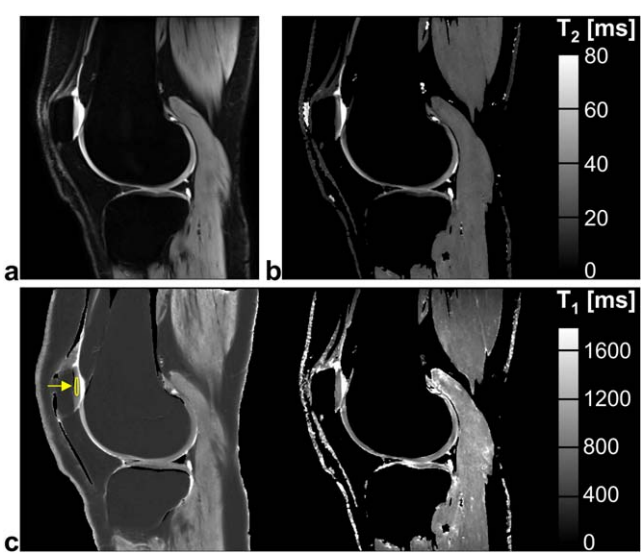

FIG. 7. (**a**) Morphological TESS image, calculated from a weighted combination of the F_0 and F_{-1} signal ($F_0 + 3 \times F_{-1}$) to accentuate the contrast between synovial fluid and cartilage, similar to DESS. (**b**) B_1-insensitive sagittal T_2 map calculated from a single TESS scan. (**c**) Sagittal TESS-T_1 map (right) is compared with a reference T_1 measurement derived from 2D multislice IR-TSE scans. TESS-T_1 is clearly affected by B_1; however, good correspondence to the IR-TSE technique can be observed for instance in the patella (region of interest indicated by the arrow). [Color figure can be viewed in the online issue, which is available at wileyonlinelibrary.com.]

Table 2
In Vivo Comparison of Spin Echo and TESS T_2 Relaxometry Data in the Knee Joint at 3 T (for Protocol Details, see "Methods" Section)

	TESS	SE[a]	SE[b]	SE[c]
		Single-echo	Multiecho	Multiecho
Tissue/[$MnCl_2$]	T_2 (ms)	T_2 (ms)	T_2 (ms)	T_2 (ms)
Cartilage[d]	27.3 ± 3.2	26.5 ± 3.2	32.9 ± 4.5	40.4 ± 5.2
Muscle[e]	26.3 ± 0.6	24.6 ± 1.1	31.1 ± 4.5	37.6 ± 4.9
0.125 mM[f]	64.2 ± 0.9	69.1 ± 0.6	84.0 ± 0.6	102.6 ± 0.7
0.250 mM[g]	34.9 ± 0.3	36.6 ± 0.1	44.4 ± 0.2	53.0 ± 0.3
0.500 mM[h]	18.0 ± 0.2	18.7 ± 0.1	23.0 ± 0.1	28.9 ± 0.1

[a]T_2 value derived based on nine single-echo SE scans using a nonlinear least-squares fit.
[b]T_2 value derived based on a multiecho SE scan (nine echoes), using a nonlinear least-squares fit. For the fit, the first echo was discarded to mitigate stimulated echo contributions.
[c]T_2 value derived based on a multiecho SE scan (nine echoes), using a nonlinear least-squares fit.
[d]For definition, see Figure 6: region of interest 1.
[e]For definition, see Figure 6: region of interest 2.
[f]For definition, see Figure 6: region of interest 3.
[g]For definition, see Figure 6: region of interest 4.
[h]For definition, see Figure 6: region of interest 5.

CONCLUSIONS

In contrast to all other existing SSFP quantification techniques, TESS offers rapid T_1 and T_2 estimation within one single scan. Moreover, quantification of T_2 with TESS is markedly insensitive to B_1. As a result, the new proposed method is of high interest for fast and reliable relaxometry in the clinical routine, especially for rapid and bias-free T_2 imaging of the musculoskeletal system at high to ultra-high field strength.

ACKNOWLEDGMENTS

We thank Nicolin Hainc for carefully reading and commenting on the manuscript.

REFERENCES

1. Carr HY. Steady-state free precession in nuclear magnetic resonance. Phys Rev 1958;112:1693–1701.
2. Bernstein MA, King KF, Zhou XJ. Handbook of MRI pulse sequences; Burlington, MA: Elsevier Academic Press; 2004.
3. Look DC, Locker DR. Time saving in measurement of NMR and EPR relaxation times. Rev Sci Instrum 1970;41:250–251.
4. Christensen KA, Grand DM, Schulman EM, Walling C. Optimal determination of relaxation times of Fourier transform nuclear magnetic resonance. Determination of spin-lattice relaxation times in chemically polarized species. J Phys Chem 1974;78:1971–1977.
5. Homer J, Beevers MS. Driven-equilibrium single-pulse observation of T_1 relaxation. A reevaluation of a rapid "new" method for determining NMR spin-lattice relaxation times. J Magn Reson 1985;63: 287–297.
6. Scheffler K, Hennig J. $T(1)$ quantification with inversion recovery TrueFISP. Magn Reson Med 2001;45:720–723.
7. Deoni SC, Rutt BK, Peters TM. Rapid combined T_1 and T_2 mapping using gradient recalled acquisition in the steady state. Magn Reson Med 2003;49:515–526.
8. Schmitt P, Griswold MA, Jakob PM, Kotas M, Gulani V, Flentje M, Haase A. Inversion recovery TrueFISP: quantification of $T(1)$, $T(2)$, and spin density. Magn Reson Med 2004;51:661–667.
9. Welsch GH, Scheffler K, Mamisch TC, Hughes T, Millington S, Deimling M, Trattnig S. Rapid estimation of cartilage T_2 based on double echo at steady state (DESS) with 3 Tesla. Magn Reson Med 2009;62: 544–549.
10. Bieri O, Scheffler K, Welsch GH, Trattnig S, Mamisch TC, Ganter C. Quantitative mapping of T_2 using partial spoiling. Magn Reson Med 2011;66:410–418.
11. Miller KL, Hargreaves BA, Gold GE, Pauly JM. Steady-state diffusion-weighted imaging of in vivo knee cartilage. Magn Reson Med 2004;51:394–398.
12. Deoni SC, Peters TM, Rutt BK. Quantitative diffusion imaging with steady-state free precession. Magn Reson Med 2004;51:428–433.
13. Bieri O, Ganter C, Welsch GH, Trattnig S, Mamisch TC, Scheffler K. Fast diffusion-weighted steady state free precession imaging of in vivo knee cartilage. Magn Reson Med 2012;67:691–700.
14. Bieri O, Ganter C, Scheffler K. Quantitative in vivo diffusion imaging of cartilage using double echo steady-state free precession. Magn Reson Med 2012;68:720–729.
15. Staroswiecki E, Granlund KL, Alley MT, Gold GE, Hargreaves BA. Simultaneous estimation of $T(2)$ and apparent diffusion coefficient in human articular cartilage in vivo with a modified three-dimensional double echo steady state (DESS) sequence at 3 T. Magn Reson Med 2012;67:1086–1096.
16. Bieri O, Mamisch TC, Trattnig S, Scheffler K. Steady state free precession magnetization transfer imaging. Magn Reson Med 2008;60:1261–1266.
17. Gloor M, Scheffler K, Bieri O. Quantitative magnetization transfer imaging using balanced SSFP. Magn Reson Med 2008;60:691–700.
18. Gloor M, Scheffler K, Bieri O. Nonbalanced SSFP-based quantitative magnetization transfer imaging. Magn Reson Med 2010;64:149–156.
19. Markl M, Alley MT, Elkins CJ, Pelc NJ. Flow effects in balanced steady state free precession imaging. Magn Reson Med 2003;50:892–903.
20. Santini F, Wetzel SG, Bock J, Markl M, Scheffler K. Time-resolved three-dimensional (3D) phase-contrast (PC) balanced steady-state free precession (bSSFP). Magn Reson Med 2009;62:966–974.
21. Stalder AF, Russe MF, Frydrychowicz A, Bock J, Hennig J, Markl M. Quantitative 2D and 3D phase contrast MRI: optimized analysis of blood flow and vessel wall parameters. Magn Reson Med 2008;60:1218–1231.
22. Yarnykh VL. Improved accuracy of variable flip angle T_1 measurements using optimal radiofrequency and gradient spoiling. In Proceedings of the 16th Annual Meeting of ISMRM, Toronto, Canada, 2008. p 234.
23. Deoni SC, Peters TM, Rutt BK. High-resolution T_1 and T_2 mapping of the brain in a clinically acceptable time with DESPOT1 and DESPOT2. Magn Reson Med 2005;53:237–241.
24. Deoni SC, Ward HA, Peters TM, Rutt BK. Rapid T_2 estimation with phase-cycled variable nutation steady-state free precession. Magn Reson Med 2004;52:435–439.
25. Mizumoto CT, Yoshitome E. Multiple echo SSFP sequences. Magn Reson Med 1991;18:244–250.
26. Vlaardingerbroeck MT, den Boer JA. Magnetic resonance imaging, 3rd ed. Berlin: Springer-Verlag; 2002. pp 423–467.
27. Hänicke W, Vogel HU. An analytical solution for the SSFP signal in MRI. Magn Reson Med 2003;49:771–775.
28. Bruder H, Fischer H, Graumann R, Deimling M. A new steady-state imaging sequence for simultaneous acquisition of two MR images with clearly different contrasts. Magn Reson Med 1988;7:35–42.
29. Press WH, Teukolsky SA, Vetterling WT, Flannery BP. Numerical recipes: the art of scientific computing. Cambridge: Cambridge University Press; 2007.
30. Lebel RM, Wilman AH. Transverse relaxometry with stimulated echo compensation. Magn Reson Med 2010;64:1005–1014.
31. Meiboom S, Gill D. Modified spin-echo method for measuring nuclear relaxation times. Rev Sci Instrum 1958;29:688–691.
32. Redpath TW, Jones RA. FADE—a new fast imaging sequence. Magn Reson Med 1988;6:224–234.
33. Bieri O, Ganter C, Scheffler K. On the fluid-tissue contrast behavior of high-resolution steady-state sequences. Magn Reson Med 2012;68:1586–1592.
34. Hardy PA, Recht MP, Piraino DW. Fat suppressed MRI of articular cartilage with a spatial-spectral excitation pulse. J Magn Reson Imaging 1998;8:1279–1287.